Int J Adv Manuf Technol (2016) 83:1487–1502
DOI 10.1007/s00170-015-7441-3

ORIGINAL ARTICLE

Tool condition monitoring by SVM classification of machined surface images in turning

Nagaraj N. Bhat[1] · **Samik Dutta**[2] · **Tarun Vashisth**[3] · **Srikanta Pal**[4] · **Surjya K. Pal**[5] · **Ranjan Sen**[2]

Received: 18 January 2013 / Accepted: 12 June 2015 / Published online: 16 August 2015

Abstract Tool condition monitoring has found its importance to meet the requirement of quality production in industries. Machined surface is directly affected by the extent of tool wear. Hence, by analyzing the machined surface, the information about the cutting tool condition can be obtained. This paper presents a novel technique for multi-classification of tool wear states using a kernel-based support vector machine (SVM) technique applied on the features extracted from the gray-level co-occurrence matrix (GLCM) of machined surface images. The tool conditions are classified into sharp, semi-dull, and dull tool states by using Gaussian and polynomial kernels. The proposed method is found to be cost-effective and reliable for online tool wear classification.

Keywords Feature selection · Turning · GLCM · Surface texture · Fisher discriminant analysis · Tool condition monitoring · Support vector machines

✉ Surjya K. Pal
skpal@mech.iitkgp.ernet.in

[1] Department of Electrical and Electronics Engineering, BIT, Mesra, Ranchi 835215, India

[2] Precision Engineering and Metrology Group, CSIR-Central Mechanical Engineering Research Institute, Durgapur, India

[3] Department of Electronics and Communication Engineering, BIT, Mesra, Ranchi 835215, India

[4] Department of Electrical Engineering, Shiv Nadar University, Dadri, Gautam Budh Nagar, Uttar Pradesh 201314, India

[5] Department of Mechanical Engineering, Indian Institute of Technology Kharagpur, Kharagpur, India

1 Introduction

In machining operations, the condition of the cutting tool plays a very important role on the quality of machined surface. The quality of machined surface and the machine tool condition degrade with the wear of the cutting tool. One proposed solution is the online monitoring of the tool condition so as to monitor the tool wear level and hence replace the cutting tool when it is worn beyond an acceptable limit. A number of techniques have been proposed for tool wear monitoring with the observation of different signals, viz., acoustic emission (AE), cutting force, tool temperature, vibration signatures, and machined surface roughness which are observable for change due to variation of the degree of tool wear [1]. The machined surface quality is directly dependent on various types of tool wears, viz., flank wear, crater wear, nose wear, fracture, and breakage. The cutting tool geometry is strongly related with the quality of machined surface [2]. Hence, analysis of the image of machined surface could provide the information about the tool wear level. The main advantages of this method over other methods of tool condition monitoring are noninvasiveness, flexibility, and inexpensiveness [3].

The detection of progressive tool wear can be possible by analyzing the machined surface images [2–10]. The texture of the machined surface has been analyzed using column projection and run length statistical (RLS) techniques [2, 4]. Bradley and Wong [5] did a performance comparison of gray-level intensity histogram, frequency spectrum analysis, and image segmentation techniques to detect progressive wear from end-milled surface images. Kang et al. [6] studied the performance of fractal analysis on end-milled surface images for progressive detection of cutting tool flank wear. A speckle pattern has been created on ground and milled surfaces, and obtained speckle pattern images have been analyzed accurately using autocorrelation technique. Finally, a

comparison of the obtained features from image analysis with measured surface roughness has been studied by Dhanasekar et al. [7]. Recently, Dutta et al. [8] performed gray-level co-occurrence matrix (GLCM) and RLS-based texture analyses on end-milled surface images taken through an optical microscope and found a high correlation between tool flank wear and extracted texture features. A Voronoi-tessellation-based texture analysis technique was applied by Datta et al. [9] on turned surface images to detect progressive wear. However, this method can only be applied on binary images, and consequently, the gray-level information was lost.

Various researchers have studied the first-order statistical texture of machined surface images for correlating the obtained features with surface roughness [10–14]. However, the quantification of spatial relationship between gray-level intensity values of image pixels is absent in first-order statistical analysis. Thus, there is a requirement to study the second-order statistical texture analysis technique, viz., the GLCM technique.

The co-occurrence information of gray-level intensities of image pixels in a particular pixel pair spacing (s) and in a particular direction (θ) has been accumulated in GLCM. Different features to describe the co-occurrence can be extracted from GLCM. The gray-level intensities are well distributed or make a proper pattern for smooth surfaces. Hence, most of the elements of GLCM lie diagonally for surface images machined by sharp tool than that by dull tool [15]. Thus, from that information, the machined surfaces obtained using sharp and dull tools can be classified with the GLCM technique. Ramana et al. [16] classify shaped, milled, and ground surface images using the extracted features from GLCM of machined surface images. Dutta et al. [17–19] have detected the progressive wear of the cutting tool from turned surface images using the GLCM technique. The proper selection of pixel pair spacing and pixel pair direction parameters also plays a very important role for obtaining accurate results of detection which have been reported in [17], and an algorithm for the method to detect the optimized pixel pair spacing parameter has been developed by Dutta et al. [18].

There are also an increasing number of pieces of research for classification of the tool conditions into two or three classes (i.e., sharp tool and dull tool or sharp tool, semi-dull tool, and dull tool). Tool wear levels can be classified based on observed trend of the feature levels obtained from different types of signals measured from machining operation. A number of methods have been proposed for classification of tool wear including neural network [20–23], fuzzy logic [24], and pattern recognition [25]. Desirable results were achieved by neural network (NN) to classify on the basis of acoustic emission and force signals in tool wear detection of a turning process [20]. Tsai et al. [23] classified the surface roughness of shaped and milled specimen by analyzing the Fourier power spectrum of shaped and milled surface images using a NN tool. The accuracy in this case depended on the sample data used for training and testing. Kohonen's self-organizing map is used to project high-dimensional data into lower dimension by preserving the input relationships. Such feature map was used for tool condition monitoring along with input feature scaling [26]. Among all the above-mentioned classification techniques, NN is the most popular technique. However, back-propagation NN (BPNN) algorithm converges very slowly and radial basis function NN (RBFNN) algorithm is less generalized algorithm due to its empirical risk minimization principle. Thus, this method is more error prone. Moreover, during machining, tool states fluctuate often leading to data error. Such nonuniform data distribution, during training or testing, adversely affects the NN algorithm.

However, the support vector machine (SVM)-based classification technique has been gaining a high research interest due to its good generalization capability for structural risk minimization principle and also its computational efficiency due to the capability for performing with lesser number of data as it considers only support vectors for classification. A Bayesian support vector regression technique for tool wear prediction has been applied to the selected features of force signal, resulting from face milling operation by Dong et al. [27]. Sun et al. [28] studied the performance of the SVM approach using a soft margin technique to classify the fresh and worn cutting tool states from the information of acoustic emission signal obtained from the cylindrical turning operation. They have utilized an automatic relevance determination (ARD) technique for feature selection. They also utilized a function considering the manufacturing loss to evaluate the misclassification rate in their tool condition monitoring (TCM) system. Sun et al. [29] improved their tool state recognition technique by classifying the tool states into three classes, viz., fresh, semi-worn, and worn states using a one-versus-one approach in the SVM technique. With another approach, Cho et al. [30] applied a support vector regression (SVR) technique for tool breakage detection using cutting force and power signal in end milling operation. They have studied that the success rate of the SVR technique was better than that of the multiple variable regression technique in their experiments. Bhattacharyya and Sanadhya [31] predicted the cutting tool wear resulting from face milling operation from force signal using an SVR technique with less than 5 % prediction error. In another work of Sun et al. [32], features from AE signal resulting from turning operation were selected by the ARD method coupled with the SVM technique. They have utilized cutting speed, feed rate, and depth of cut as input features. Using this approach, the accuracy of classification of tool states has been improved to 85 %. Shi and Gindy [33] studied a good prediction performance by applying a least squares (LS) SVM technique to predict the wear of a broaching tool from the force signal information. Salgado and Alonso [34] applied the LS-SVM

technique for its better computational ability than standard SVM for prediction of tool wear from the information of force and current signals resulting from a turning operation. Study of much better generalization capability of LS-SVM than that of artificial NN (ANN) has been reflected in their work. Hsueh and Yang [35] used a grid search technique for optimum selection of penalty factor used in their SVM method for classifying the damaged and undamaged tool states from force information resulting from a face milling operation. Chiu and Guao [36] predicted the four states of a CBN grinding tool using SVM on AE signal with 85 % accuracy. Karacal et al. [37] proposed an approach for the classification of coated carbide tool condition using the SVM technique applied on the smell signal resulting from chemical reaction during machining. Jiang [38] predicted surface roughness of milled specimens using the LS-SVM technique with less than 8 % error. Cho et al. [39] predicted and classified the condition of a milling cutter into five classes of wear, viz., fracture, breakage, fresh, semi-worn, and worn states by combining the recognition results of multi-layer perceptron NN, RBFNN, and SVM technique on the AE, force, and vibration signals with ensemble accuracy of 97 %. The SVM technique outperformed others, according to their study, with the highest accuracy of 95.9 %. Huang et al. [40] predicted the condition of the ball nose end milling cutter by applying a different kernel-based SVR technique on force signal and suggested that the polynomial kernel was showing the best performance. Elangovan et al. [41] compared the performance of decision tree, Naïve Bayes, Bayes Net, ν-support vector classification (SVC), and C-SVC for classifying the fresh tool, semi-worn tool, worn tool, and broken tool using vibration signal resulting from a turning operation. According to their study, C-SVC outperformed other techniques for classification. Also, the polynomial kernel of degree 2 used in the SVM technique was proved to be computationally efficient and RBF kernel was efficient in terms of classification accuracy, according to their study. Brezak et al. [42] used a hybrid tool wear estimation technique using analytic fuzzy classifier for tool classification and an RBF-kernel-based SVM technique for wear estimation using feed force, feed current, and AE signal resulting from end milling operation. Thus, a dynamic feature selection process has been accomplished in their method. A performance comparison of *k*-means clustering SVM, LS-SVM, spider SVM, and ANN methods for prediction of surface roughness for turning austenitic stainless steel material has been studied by Çaydaş and Ekici [43]. Spider SVM was most successful compared to ANN, as claimed by them.

However, the pieces of research associated with SVM and TCM were done using either contact methods or one-dimensional signal. Nowadays, there is a greater need for noninvasive TCM for multi-classification of cutting tool wear states. Research involving SVM on the features extracted from the machined surface texture images has not yet been performed. A method for multi-classification of tool wear states using the kernel-based SVM technique applied on the extracted features from GLCM of machined surface images has been proposed in this work. In the present scenario, there is a great demand for the application of image processing in tool condition monitoring due to its noninvasiveness, cost-effectiveness, and flexibility as compared to any other techniques.

There are a number of applications of SVM for classification using GLCM features in the field of medical science and remote sensing. In the field of medical science, breast tumors were well segmented and classified from the mammograms by incorporating SVM classifier on GLCM features by Eddaoudi et al. [44]. Rode and Patil [45] classified the brain MRI of a multiple sclerosis patient and that of a healthy person using SVM and ANN classifier on the GLCM features extracted from MRI images. Paneque-Gálvez et al. [46] studied that the SVM technique outperformed other classification methods, viz., parametric (ML), nonparametric (*k*-nearest neighborhood), and hybrid classifier for the texture classification of different land cover images. They have used homogeneity of GLCM as a feature. Pawade et al. [47] classified different Brodatz textures using different kernel-based SVM classifiers applied on the feature data extracted from GLCM. They have found that the radial basis function and exponential radial basis function kernels outperformed the other kernels, viz., second-degree polynomial, sigmoid, and odd-order B-spline. Recent pieces of research show that SVM has become popular in learning methods due to its excellent generalization ability than any other traditional methods, like ANN.

However, there are very few studies discussing the applications of SVM in TCM. No research is reported in the application of SVM in online TCM by machined surface texture analysis. In this paper, the condition of the cutting tool for sharp, semi-dull, and dull states has been classified by the kernel-based SVM technique using the GLCM features extracted from machined surface images.

Table 1 Experimental setup

Machine tool	NH-26 lathe
Cutting tool insert	SNMG 120408-QM
Camera	Genie HM1024
Tele lens with polarizer	Navitar zoom lens with macro-zoom, focal length 18–108 mm
Image acquisition software	SAPERA LT
Illumination system	DC-regulated fiber-optic-guided light (Navitar)

Table 2 Machining conditions

Machining conditions	Cutting speed (m/min)	Feed rate (mm/rev)	Depth of cut (mm)
1	100	0.20	2
2	100	0.24	0.5
3	100	0.16	0.5
4	100	0.32	0.5

2 Experimental setup

In this work, C-50 steel workpiece material has been turned with uncoated carbide inserts in dry cutting condition. The carbon and sulfur percentage of the material has been analyzed using a carbon-sulfur combustion analyzer (Horiba EMIA 320 V). In this method of analysis, the chips obtained from the cutting operation are heated through a high-frequency induction furnace, and the filtered dust obtained by heating the chip samples is passed through a dehydrator. Finally, an infrared detector is detecting the carbon and sulfur percentage from obtained CO, CO_2, and SO_2. The carbon and sulfur percentage of the work material is 0.51 and 0.043 %, respectively. After cutting full-length job (500-mm length), the machined surfaces were imaged as 1024×768-pixel gray-level digital images using an area scan monochrome camera connected to a computer equipped with image acquisition capability at five different positions on the machined surface. The images of the machined surface were taken on machine tool by illuminating the machined surface by a DC-regulated fiber-optic-guided illuminator. The position of the camera and the lighting source was made fixed with respect to the workpiece surface. The corresponding average flank wear ($VB_{average}$) of the insert was also measured using an Olympus microscope with ×10 magnification equipped with image acquisition software, Olympus image analyzer. Simultaneously, the average surface roughness (R_a) of turned surface was also measured at the corresponding positions. Table 1 summarizes the experimental setup of the turning operations applied to C-50 steel workpiece and image acquisition hardware. Table 2 summarizes the machining conditions. The experimental setup is shown in Fig. 1. Each of the images was cropped to 210×210-pixel image before processing. All image processing were done in MATLAB® (version 7.8.0.347 R2009a) environment.

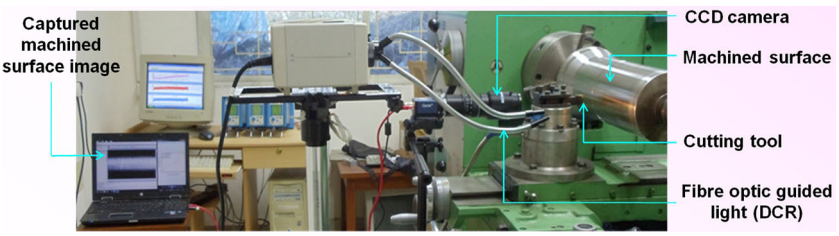

Fig. 1 Experimental setup

3 Methodology

In this work, the machined surface images have been preprocessed using a contrast-limited adaptive histogram equalization (CLAHE) technique for overcoming the effects on images due to nonuniform illumination. And then, the preprocessed images have been analyzed by using GLCM technique. Fifteen features have been extracted from the GLCM of each image and a Fisher discrimination technique has been applied for feature selection. The selected features have been used as the input to SVM for classification of tool wear states as sharp ($VB_{average}$<100 μm), semi-dull (100 μm <$VB_{average}$<300 μm), and dull ($VB_{average}$>300 μm) tool states [48].

3.1 Pre-processing

The images of the machined surface were suffering from non-uniform illumination due to a small change of lighting at the time of image acquisition. Thus, a preprocessing step is required to distribute the same level of illuminations in machined surface images. So, to overcome this problem, the machined surface images were preprocessed by adaptive histogram equalization vis-à-vis enhancement of the contrast to bring out more details using the CLAHE technique in this work. Histogram equalization (HE) transformed a low-contrast image into a high-contrast image [49]. Adaptive histogram equalization (AHE) technique improves the HE technique by equalizing the histograms of distinct sections of an image and by redistributing the gray-level uniformly. However, there is a chance of over-amplification of noises in AHE. CLAHE limits this over-amplification of noise by limiting the contrast of an image [50].The images of the turned surface before and after applying the CLAHE are shown in Fig. 2a, b, respectively. The corresponding histograms of Fig. 2a, b are also shown in Fig. 2c, d, respectively. From the histogram of Fig. 2a, b, it can be inferred that the pixel intensities are distributed uniformly in Fig. 2b providing a clear contrast of the surface image, whereas in Fig. 2a the pixel intensity is distributed more toward white.

3.2 Gray-level co-occurrence technique

Since, machined surface images are periodic texture images, a statistical texture analysis using gray-level co-occurrence

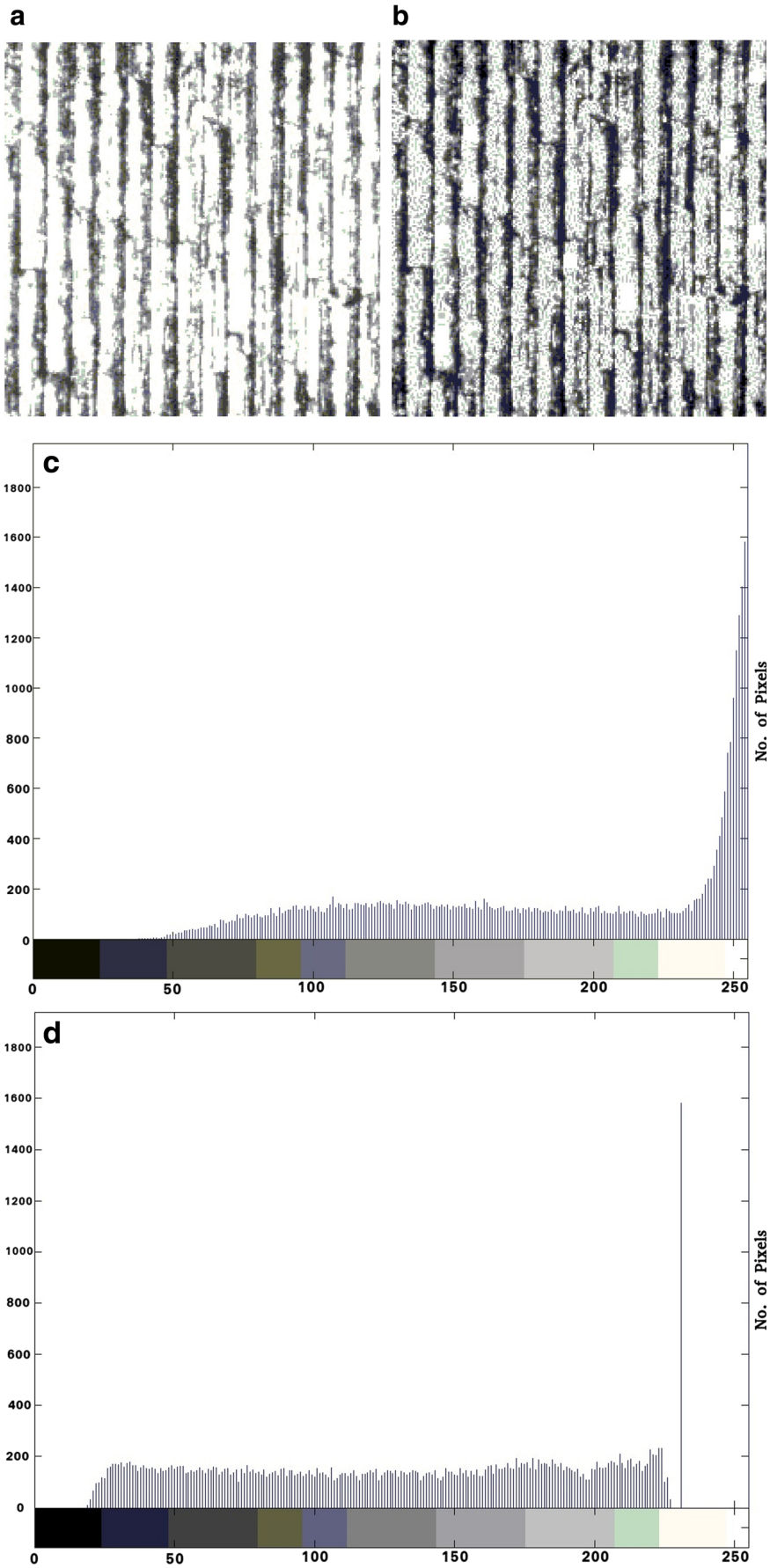

Fig. 2 **a** Raw image, **b** corresponding preprocessed image, **c** histogram of original image, and **d** histogram of preprocessed image

technique has been incorporated in this study. The GLCM technique has been proposed by Haralick et al. [51]. Each element of the GLCM of an image is the number of co-occurrence of corresponding pixel pair in a specified spacing (s) and a specified direction (θ). Formally, it can be shown in Eq. (1):

$$GLCM(i,j)_{s,\theta} = |\{(p_1,p_2)|I(p_1) = i, I(p_2) = j\}| \quad (1)$$

where $(p_1,p_2) \in M \times N$ and p_2 is at the direction of θ at a spacing s from p_1. Here, p_1 and p_2 are representing the positions of two image pixels. $|.|$ represents the cardinality of a set. As the feed marks of the turned surface images are lying vertically, the θ value is taken in this work as 0°. The construction process of GLCM from an original image fragment matrix is shown in Fig. 3a, b.

The co-occurrence of nine and seven gray-level intensity values (Fig. 3a) is occurring for three times with spacing 1 and direction 0°, which is shown with a circle in the GLCM of the image fragment shown in Fig. 3b. This can also be stated as the co-occurrence of 1 pixel in the x direction and 0 pixel in the y direction. In this case, the selection of appropriate s for constructing the GLCM is important as the repetitive occurrence of feed marks in turned surface images [18]. The appropriate pixel pair spacing (s) values for different machining conditions are calculated by using the technique applied by Dutta et al. [18] and are given in Table 3.

After constructing the GLCM, 15 features, namely, *contrast(F1)*, *energy(F2)*, *correlation(F3)*, *homogeneity(F4)*, *entropy(F5)*, *inverse diagonal moment (IDM)(F6)*, *dissimilarity(F7)*, *mean(F8)*, *variance(F9)*, *maximum probability(F10)*, *diagonal moment(F11)*, *second diagonal moment(F12)*, *coefficient of variation(F13)*, *cluster shade(F14)* and *cluster prominence(F15)*, have been extracted [52, 53]. The normalized feature values for both raw and preprocessed images of 15 features were extracted for all four machining conditions. The feature values of machining condition 1 for the preprocessed image are shown in Table 4.

3.3 Feature selection using Fisher discriminant ratio analysis

The 15 parameters extracted by the GLCM technique provide a wide range of classification, but some features may be too noisy resulting in poor classification. The presence of large amount of data in every feature, using all the features for classification, increases the computational time. This is practically not feasible in real-time application for online monitoring. Hence, it is necessary to select prominent features which provide significant details of the image and which are less affected by noise and other variations. The extracted features were analyzed using Fisher's discriminant ratio (FDR) analysis. FDR is commonly employed to quantify the discriminatory power of individual features between two equiprobable classes [54]. In other words, it is independent of the type of class distribution. The main reasons for selecting FDR analysis over other methods are as follows:

- FDR provides an optimal representation in terms of maximizing the separation among several classes [55].
- FDR is simple and computationally fast.
- It focuses mainly on the statistical distribution of data rather than other methods which focus on the variables used in order to investigate the differences between groups and create synthetic variables.

The dataset of every machining condition was divided into two classes, the first half of the data was assigned as class 1 (sharp tool dominance), and the next half of the data was assigned as class 2 (dull tool dominance). Let m_1 and m_2 be the respective mean values and ${\sigma_1}^2$ and ${\sigma_2}^2$ the respective variances associated with the values of a feature in two classes. The FDR is defined by Eq. (2) [54].

$$FDR = \frac{(m_1 - m_2)^2}{({\sigma_1}^2 + {\sigma_2}^2)} \quad (2)$$

It can be observed from Eq. (2) that features having large mean difference and small variance in each class get a higher value. Thus, the higher the ratio of a feature, the better it is for classification. FDR was calculated for each feature extracted from both raw and preprocessed images for all four machining conditions. The obtained FDR values for raw and preprocessed images are given in Tables 5 and 6, respectively. M1, M2, M3, and M4 refer to the machining

Table 3 Appropriate s values corresponding to the experiment numbers

Machining conditions (as stated in Table 2)	Appropriate s (in pixel)
1	10
2	16
3	10
4	19

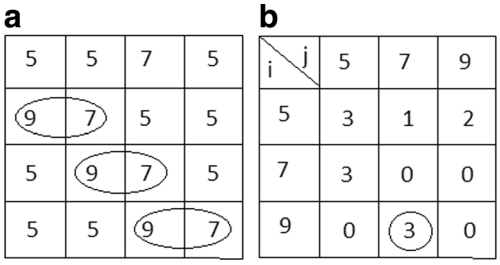

Fig. 3 **a** An image fragment and **b** corresponding GLCM

Table 4 Fifteen features extracted for machining condition M1 of preprocessed image

Time/Tool condition (min)	$VB_{average}$ (μm)	F1	F2	F3	F4	F5	F6	F7	F8	F9	F10	F11	F12	F13	F14	F15
2	75	0.0322	0.3700	0.9590	0.7851	0.0853	0.706	0.0453	0.7631	0.5928	0.3927	0.0486	0.0453	0.1863	0.2729	0.3645
		0.0274	0.3142	0.957	0.7399	0	0.6582	0.0508	0.7273	0.5341	0.3204	0.0290	0.0508	0.1754	0.3465	0.4537
Sharp		0.038	0.2759	0.9404	0.7493	0.1651	0.684	0.0600	0.6201	0.4712	0.4120	0.0942	0.0600	0.2047	0.5873	0.6249
		0.0538	0.5852	0.9549	0.782	0.1010	0.7391	0.0753	0.7801	0.7350	0.6048	0.0604	0.0753	0.2524	0.2284	0.3334
		0	1	1	1	0.0616	1	0	0.8256	0.7504	1	0	0	0.2337	0.1497	0.2588
4	100	0.2086	0.0334	0.7587	0.7505	0.7531	0.3321	0.1327	0.2200	0.2886	0.0072	0.4159	0.2446	0.3728	0.9842	0.968
		0.2145	0.0489	0.7554	0.6459	0.6487	0.3460	0.1208	0.4357	0.3014	0.0345	0.3751	0.2623	0.2236	0.7754	0.7898
Sharp		0.2500	0.0565	0.7460	0.7350	0.7218	0.3338	0.137	0.4820	0.429	0.0763	0.4135	0.2923	0.2693	0.7738	0.7890
		0.2200	0.0363	0.7294	0.7836	0.7120	0.2678	0.1706	0.4741	0.1929	0.0136	0.4155	0.2778	0.1335	0.6925	0.7462
		0.2728	0.0332	0.6978	0.6806	0.7549	0.2763	0.1530	0.3900	0.2873	0.0072	0.4649	0.3204	0.2460	0.8313	0.8511
6	129	0.0969	0.0614	0.8629	0.5582	0.5074	0.4495	0.2446	0.486	0.2802	0.0329	0.239	0.1327	0.1779	0.6981	0.7482
		0.0831	0.0572	0.8675	0.5671	0.4819	0.4491	0.2623	0.4324	0.2208	0.0345	0.2386	0.1208	0.1768	0.7822	0.8042
Sharp		0.0936	0.0614	0.8524	0.5155	0.4809	0.3879	0.2923	0.4406	0.1891	0.0393	0.2408	0.13	0.1523	0.765	0.8004
		0.1204	0.0473	0.7926	0.4484	0.5029	0.3154	0.2778	0.3977	0	0.0032	0.2777	0.1706	0.0637	0.8001	0.8244
		0.1178	0.0704	0.8604	0.5312	0.3922	0.4124	0.3204	0.4958	0.3976	0.0393	0.2216	0.1530	0.2413	0.572	0.651
10	169	0.2867	0.0305	0.6921	0.405	0.8860	0.3022	0.3087	0.6093	0.3231	0.0176	0.5245	0.3087	0.1273	0.5136	0.5821
		0.3090	0.0560	0.6631	0.4057	0.7945	0.3059	0.3324	0.7361	0.2847	0.0281	0.4866	0.3324	0.0351	0.4991	0.5612
Sharp		0.3423	0.0168	0.6512	0.4181	0.9448	0.2266	0.3816	0.5166	0.3726	0.0056	0.6268	0.3816	0.2130	0.518	0.6029
		0.2771	0.0087	0.6562	0.3650	0.9698	0.2528	0.3083	0.1901	0.1173	0.0008	0.6110	0.3083	0.2818	0.734	0.7907
		0.2362	0.0100	0.6904	0.368	0.9540	0.2578	0.2851	0.2965	0.085	0.0008	0.5792	0.2851	0.1834	0.6979	0.7475
17	186	0.5389	0.3495	0.5627	0.4596	0.6867	0.5577	0.4770	1	0.7439	0.4329	0.4208	0.4770	0.1347	0	0
		0.6438	0.2693	0.4525	0.4124	0.6988	0.4154	0.5916	0.9863	0.6440	0.4152	0.4969	0.5916	0.0921	0.1642	0.2047
Semi-dull		0.5538	0.0695	0.457	0.2834	0.8035	0.2092	0.5355	0.8960	0.3726	0.0313	0.5633	0.5355	0	0.2516	0.3423
		0.5325	0.0670	0.4716	0.3600	0.8137	0.2906	0.5059	0.837	0.3535	0.065	0.5649	0.5059	0.0192	0.359	0.4305
		0.6142	0.0816	0.4579	0.3330	0.8198	0.2745	0.5680	0.8494	0.5691	0.065	0.5827	0.5680	0.1255	0.229	0.2790
19	206	0.6864	0.0139	0.3478	0.3058	0.9626	0.1542	0.5682	0.4203	0.4095	0.0128	0.7893	0.6682	0.2999	0.6781	0.7132
		0.6534	0.0139	0.283	0.2975	0.9594	0.1347	0.5498	0.472	0.1337	0.0048	0.7963	0.4498	0.0992	0.6618	0.7082
Semi-dull		0.7078	0.0302	0.2932	0.2837	0.9315	0.1288	0.5872	0.5461	0.3053	0.047	0.7563	0.6872	0.1551	0.6428	0.6954
		0.7448	0.0830	0.3493	0.2803	0.9063	0.1357	0.6162	0.6422	0.580	0.0730	0.6896	0.5162	0.2525	0.5755	0.6186
		0.7092	0.0363	0.3081	0.2853	0.908	0.1429	0.5988	0.5314	0.3521	0.0257	0.7328	0.6588	0.191	0.6893	0.7421
21	245	1	0.0320	0.0231	0.2896	0.7807	0	0.6215	0.3800	0.3143	0.0056	0.8270	0.712	0.2696	0.8384	0.8319
		0.8819	0.0298	0	0.2621	0.7670	0.0140	0.6131	0.1489	0.0200	0	0.8030	0.6131	0.2475	0.8482	0.8361
Semi-dull		0.9831	0.0381	0.009	0.2415	0.704	0.0092	0.6835	0.375	0.2498	0.0040	0.7779	0.5535	0.2330	0.8455	0.832
		0.944	0.0323	0.0528	0.2542	0.783	0.0068	0.6054	0.3836	0.2640	0.0064	0.8044	0.6554	0.2360	0.8553	0.8408
		0.8987	0.0251	0.0939	0.2501	0.8332	0.0374	0.6050	0.3215	0.2575	0.0048	0.8156	0.6050	0.2757	0.8603	0.843
23	270	0.5952	0.0163	0.4390	0.2389	0.9999	0.1939	0.6006	0.3197	0.4401	0.0618	0.8256	0.6006	0.3931	0.9145	0.8941

Table 4 (continued)

Time/Tool condition (min)	$VB_{average}$ (μm)	F1	F2	F3	F4	F5	F6	F7	F8	F9	F10	F11	F12	F13	F14	F15
		0.5613	0	0.4481	0.2795	0.9928	0.2078	0.5457	0.245	0.3642	0.022	0.8534	0.5457	0.4023	0.8522	0.8583
Dull		0.6435	0.0143	0.4172	0.2512	1	0.1932	0.6290	0.2114	0.5135	0.0385	0.8474	0.6290	0.529	0.9391	0.9403
		0.6617	0.0235	0.412	0.2150	0.9986	0.1557	0.6419	0.3199	0.5522	0.0265	0.8236	0.6419	0.4643	0.7808	0.8152
		0.7797	0.1292	0.361	0.2581	0.9617	0.2523	0.7386	0.5504	0.721	0.2481	0.7442	0.7386	0.3937	0.7903	0.791
25	294	0.6965	0.1115	0.4728	0.2952	0.9656	0.2781	0.6658	0.6296	0.8974	0.1887	0.7321	0.6658	0.4389	0.6245	0.6542
		0.7287	0.1567	0.4401	0.2434	0.9343	0.3479	0.6862	0.7349	0.8657	0.2915	0.7151	0.6862	0.3507	0.6247	0.6330
Dull		0.7117	0.1552	0.4635	0.2192	0.9574	0.3300	0.6875	0.6476	0.9079	0.3108	0.7289	0.6875	0.4323	0.6008	0.628
		0.7085	0.1429	0.4872	0.2194	0.9611	0.289	0.6580	0.6755	1	0.177	0.702	0.6580	0.4641	0.5638	0.5795
		0.6230	0.2963	0.5397	0.241	0.9418	0.4322	0.5767	0.7268	0.9440	0.4345	0.6354	0.5767	0.3986	0.6071	0.5715
30	340	0.8365	0.0051	0.3222	0.172	0.9696	0.123	0.771	0.0537	0.7462	0.0337	1	0.771	0.8431	0.8840	0.9238
		0.8517	0.0136	0.3464	0.164	0.9768	0.1267	0.7880	0.1049	0.8738	0.0497	0.9926	0.7880	0.8783	0.8763	0.9167
Dull		0.8140	0.0044	0.3331	0.1684	0.9854	0.1243	0.7602	0.0278	0.7209	0.0385	0.9823	0.7602	0.8531	1	1
		0.9101	0.0296	0.3246	0.1694	0.9922	0.1243	0.8176	0.0492	0.9582	0.0353	0.959	0.8176	1	0.9257	0.9697
		0.8767	0.0197	0.318	0.1798	0.989	0.131	0.7974	0	0.8436	0.0321	0.9616	0.7974	0.9741	0.980	0.9901

conditions 1, 2, 3, and 4 mentioned in Table 2, respectively. For convenience, all the features are ranked in a descending order. Investigating the results obtained by FDR analysis, it was observed that only few features are stable in all the machining conditions for both raw and preprocessed images. Initially, those features, whose FDR values are greater than one, are selected.

Analysis of features selected in raw data reveals that features like *contrast*, *IDM*, *CSH*, and *CPM* show a highly varied difference in the ratios and ranking of FDR analysis. *Contrast* varies from 13.42 for M1 to 1.37 for M4, which is a significantly large difference. *IDM* also varies from 8.29 for M4 to 1.21 for M1; *CSH* shows a variation from 12.0 for M4 to 0.58 for M1. Similarly, *CPM* varies from 10 for M4 to 0.44 for M1. *Cor*, *energy*, *Coeff*, and *Var* are the lowest ranked feature in most of the cases (M1, M3, and M4). *Entropy* does not show such a high difference in the FDR values but is tending to one in most of the cases (M1, M3, and M4). Also, for all the four machining conditions, *MPR* shows high ratio for M2, M3, and M4 but less than 1 for M1. This analysis reveals that the features like CSH and CPM are sensitive to external noise and vary with the experimental conditions. Thus, the features which are relatively stable in all the four machining conditions are *DiagM*, *SDiagM*, *Dis*, *Homog*, and *Mean*. *DiagM*, *SDiagM*, and *Dis* did not show significant difference in the FDR ratio. *DiagM* varies from maximum of 7.8 for M2 to minimum of 6.07 for M1. *SDiagm* varies from 8.1 for M1 to minimum of 6.4 for M2. *Dis* varies from 7.2 for M3 to 4.9 for M4. *Homog* shows a variation from 8.2 to 5.8. *Mean* shows a variation from 6.9 for M3 to 1.5 for M1, which was significant but tending to 1. Hence, *Mean* is the least considerable feature out of selected five features.

The FDR analysis of preprocessed image shows that *CSH* and *CPM* are the top ranked features in M3, M1, and M4. *DiagM* and *SDiagM* do not show much variation in FDR ratio. *DiagM* is also a predominant feature for all four machining conditions as compared to *CSH*. Also, FDR of *DIS* varies from maximum of 6.9 for M3 to minimum of 4.9 for M4. Similarly, *Mpr* and *Homogeneity* do not show a much variation in FDR values. Again, *Mean* is the least feature to be considered out of the other features. *Var*, *Coeff*, and *energy* are the least ranked features in most of the cases. *Entropy* shows a high variation from 5.2 for M2 to 0.8 for M3. Also, *Contrast* varies from 5.5 for M1 to 1.1 for M4. Hence, *CSH*, *CPM*, *Diagm*, *SDiagm*, *DIS*, *MPR*, *Homog*, and *Mean* are the acceptable features in this case.

From Table 6, it can be observed that the acceptability of the number of features in the case of preprocessed images has increased as compared to the case of raw images. This is acceptable as the quality of the image is increased due to preprocessing. Within the common features selected in FDR analysis of raw image, *CSH*,

Table 5 FDR analysis of raw images

Machining condition 1 (M1)		Machining condition 2 (M2)		Machining condition 3 (M3)		Machining condition 4 (M4)	
Features	FDR	Features	FDR	Features	FDR	Features	FDR
Contrast	13.4209	*Contrast*	8.8825	*Me*	9.8037	*Me*	13.9244
SDiagM	8.1186	*Me*	8.7982	*CPM*	8.9869	*CSH*	12.0523
DIS	7.295	*Diagm*	7.8404	*Diagm*	6.4306	*Mpr*	10.6968
Me	6.194	*SDiagM*	7.6859	*SDiagM*	6.4089	*CPM*	10.0658
Diagm	6.0755	*Homog*	6.775	*Homog*	5.9391	*IDM*	8.2948
Homog	5.8437	*IDM*	5.6137	*IDM*	5.884	*Homog*	8.2886
Entropy	1.9606	*Mpr*	5.6051	*Mpr*	5.8561	*SDiagM*	6.6325
Coeff	1.5971	*Energy*	4.988	*DIS*	5.8359	*Diagm*	6.3002
IDM	1.2193	*Entropy*	4.6659	*CSH*	5.8359	*Energy*	4.7665
Var	0.8621	*DIS*	4.6659	*Contrast*	3.7643	*DIS*	4.5555
CSH	0.582	*CSH*	3.7446	*Coeff*	3.252	*Coeff*	3.0639
CPM	0.4454	*CPM*	2.8609	*Energy*	3.1086	*Var*	2.1959
Cor	0.4002	*Cor*	1.8373	*Cor*	2.9353	*Entropy*	1.8564
Energy	0.159	*Coeff*	1.3514	*Entropy*	1.2865	*Cor*	1.3742
Mpr	0.0378	*Var*	0.5088	*Var*	0.5398	*Contrast*	1.3742

CPM, and *Mpr* were also prominent. This analysis shows that these three features are sensitive to illuminations as they became predominant only after preprocessing since features like *CSH* depend on the asymmetry of pixel intensity distribution which varies widely with the illumination.

The four main features used for classification are *diagonal moment*, *second diagonal moment*, *dissimilarity*, and *homogeneity*. These features are common among raw and preprocessed images and are considered as the significant features for classification. Since, *mean* had an FDR closer to 1 in some cases, it is not considered for classification. These features are stable in both the cases, which implies that they are least affected by noise. Thus, the number of features is reduced from 15 to 4. This saves a lot of computational time and at the same time increases the classification efficiency by removing the noisy features.

Table 6 FDR analysis of preprocessed image

Machining condition 1 (M1)		Machining condition 2 (M2)		Machining condition 3 (M3)		Machining condition 4 (M4)	
Features	FDR	Features	FDR	Features	FDR	Features	FDR
CSH	11.1386	*Diagm*	7.9556	*CPM*	14.466	*CSH*	14.67
CPM	8.241	*CSH*	7.503	*CSH*	13.6841	*CPM*	12.343
SDiagM	7.3651	*SDiagM*	7.4126	*DIS*	6.983	*Homog*	7.839
Diagm	5.5669	*Homog*	5.6981	*SDiagM*	6.5985	*Diagm*	7.7944
Cor	5.5134	*Mpr*	5.6415	*Diagm*	6.5941	*IDM*	7.6882
DIS	5.0407	*IDM*	5.6227	*Homog*	6.2995	*Var*	7.5669
Mpr	4.8345	*DIS*	5.4793	*IDM*	6.2598	*Mpr*	6.4861
Homog	4.4268	*Entropy*	5.2293	*Mpr*	6.242	*SDiagM*	4.9517
Me	1.5098	*CPM*	4.9979	*Me*	6.1892	*DIS*	4.9517
IDM	1.3211	*Energy*	4.9739	*Contrast*	5.644	*Entropy*	4.9514
Entropy	1.243	*Contrast*	3.8457	*Coeff*	3.6971	*Me*	4.2552
Contrast	0.7652	*Me*	2.9552	*Energy*	3.5219	*Coeff*	3.7844
Var	0.3963	*Cor*	2.6093	*Cor*	3.199	*Energy*	3.4507
Energy	0.1485	*Coeff*	0.9366	*Var*	1.2216	*Cor*	1.1925
Coeff	0.097	*Var*	0.5567	*Entropy*	0.8659	*Contrastn*	0.7091

3.4 Support vector machine

SVM discriminates the data points into two classes. Each data point belongs to one of the two classes separated by a linear classifier with a hyperplane [56]. Figure 4a shows different linear classifiers for separating the data points into two classes. It is necessary to choose the hyperplane with maximum margin between two classes for best classification. SVM picks the hyperplane with maximum margin to correctly classify the testing data points. This maximum margin hyperplane is determined by a subset of data points called support vectors.

Figure 4b shows the maximum margin hyperplane based on support vectors (encircled data points). Hence, only a few data points (support vectors) are required to determine the hyperplane, thereby making it computationally efficient. A brief discussion on SVM is provided.

For a dataset:

$$D = \{(x_i, y_i)\} \quad [i = 1, 2, 3 \ldots l] \; where \; y_i \in \{-1, +1\}$$

The hyperplane $f(x)=0$ that separates the data is given by

$$f(x) = w^T x + b = \sum_{j=1}^{M} w_i x_j + b = 0 \tag{3}$$

where w is the M dimension vector and b is the scalar used to define the position of separating hyperplane.

Thus, the width of the margin is $\frac{2}{|w|}$, maximizing $\frac{2}{|w|}$, which implies minimizing $\frac{1}{2}\|w\|^2$.

Taking into account the noise with slack variables, ξ_i (Fig. 4c) and the penalty for error, C, the best hyperplane can be obtained using quadratic optimization by minimizing

$$\frac{1}{2}w^2 + C\sum_{i=1}^{M}\xi_i \tag{4}$$

$$\text{subjected to } \left\{y_i\left(\left(w^T x + b\right) \geq 1 - \xi_i\right)\right\}(i = 1, 2 \ldots M)\xi_i \geq 0$$

where ξ_i is the distance between the margin and the data points, x_i, that lie on the wrong side of the margin. Simplifying the above solution using Lagrangian dual problem, the decision function is

$$f(x) = \text{sign}\left(\sum_{i,j=1}^{M} \alpha_i y_i x_i x_j + b\right) \tag{5}$$

where α_i is the Lagrangian multiplier.

A nonlinear classification can be carried out by mapping function $\Phi(x_i)$ to map the input space into a higher dimensional space, so that the nonlinear hyperplane becomes linear. Hence, kernel trick $K(x_i, x_j)$ is employed to calculate the equivalent kernel value in the input space (Fig. 4d).

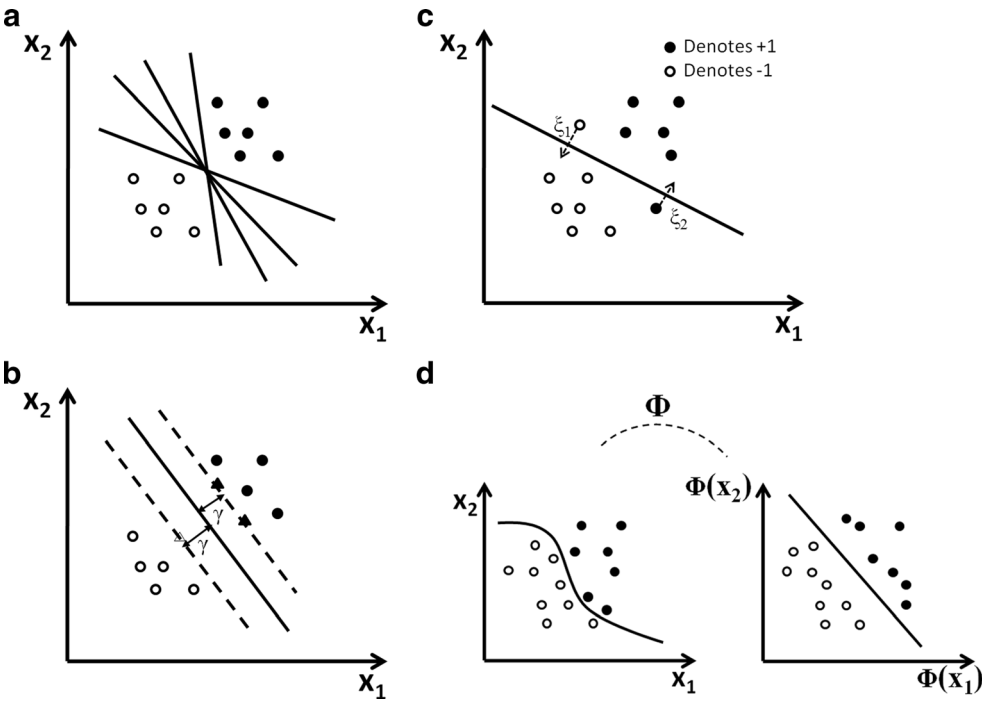

Fig. 4 **a** Linear classifier for two classes, **b** hyperplane based on support vectors, **c** classification with error variables, and **d** nonlinear kernel transformation

$$K(x_i, x_j) = \Phi(x_i)^T \Phi(x_j) \quad (6)$$

Gaussian and polynomial kernels were used in this work. Their functions are given by

- polynomial: $K(x_i,x_j)=(1+ x_i^T x_j)^p$, p is the degree of polynomial
- Gaussian: $K(x_i, x_j) = \exp\left(-\frac{||x_i - x_j||^2}{2\sigma^2}\right)$

To classify the data into three sets of classes, a one versus one approach with a Max-Win voting strategy is employed here. This approach constructs one binary classifier for every pair of distinct classes. Hence, for K number of classes, $\frac{K(K-1)}{2}$ binary classifiers are constructed where each one is trained on data from two classes. Since this approach is more suitable for practical application and is computationally fast, we have employed this approach in our multi-classification for training data from ith and jth classes according to binary classification problem.

According to the Max-Win strategy, if sign sign$((w)^T\Phi(x_i)+b)$ says that X is present in the ith class, then the vote for the ith class is added by one. Else, the jth class is increased by one. Thus, X is predicted in the class having the largest vote.

4 Results and discussion

The four features selected among all other features for classification of tool into sharp, semi-dull, and dull tool classes are *diagonal moment*, *second diagonal moment*, *dissimilarity*, and *homogeneity*. The variations of these features with time are shown in Fig. 5a, b, c, d). It can be observed that three features, namely, *diagonal*

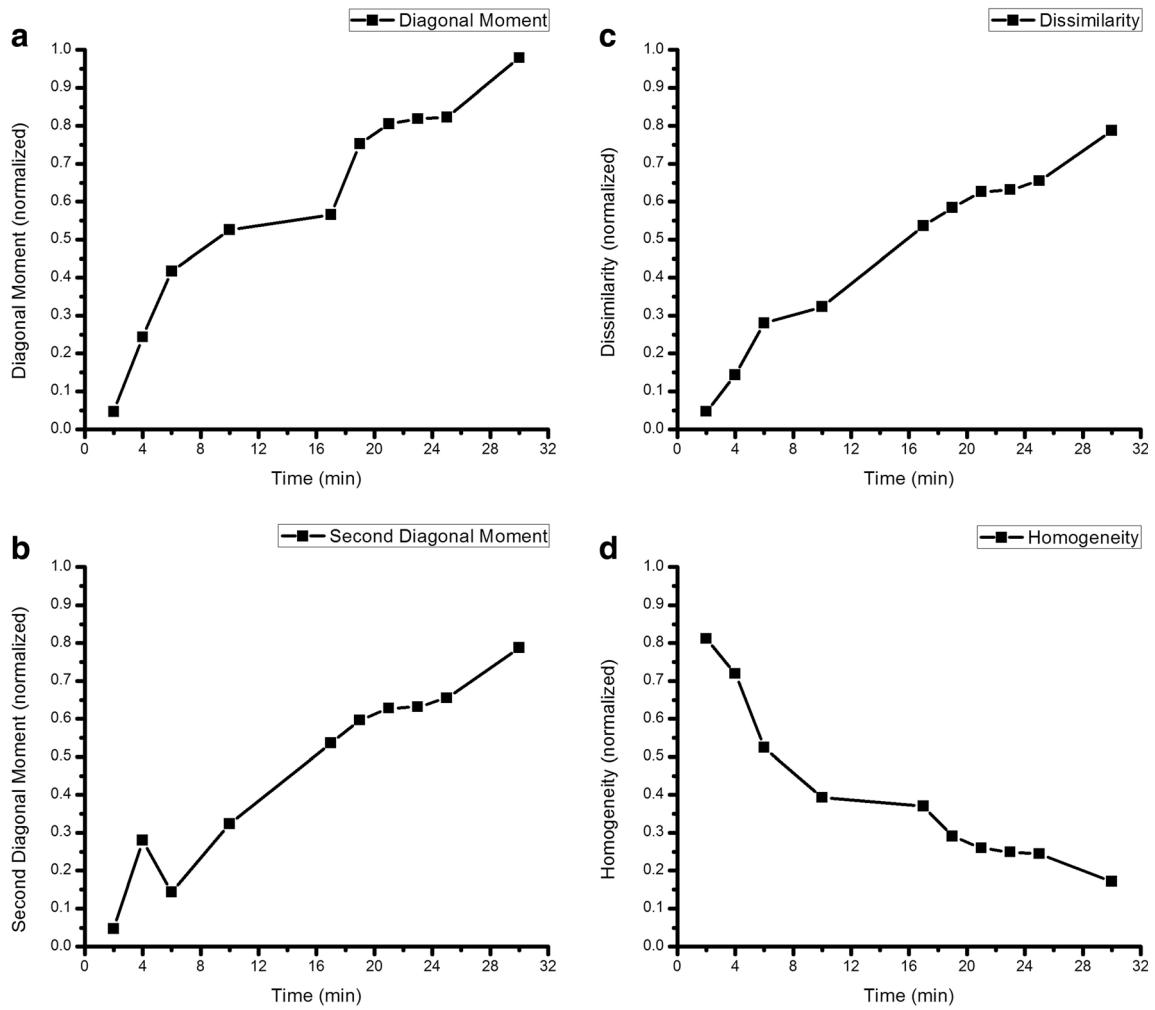

Fig. 5 **a** Variation of DiagM with time, **b** variation of SDiagM with time, **c** variation of Dis with time, and **d** variation of homo with time

moment, *second diagonal moment*, and *dissimilarity* increase with machining time, whereas *homogeneity* decreases with machining time.

The four features considered for tool wear classification would give an idea of tool state. The feature data of the preprocessed image are used for classification purpose as it is devoid of noise. Figure 6a, b, c, d) shows feature state plots for all machining conditions.

Investigating the above feature state plots for all four machining conditions, it can be observed that a certain amount of noise or wrong classification data is present. Classification data 9 in M1 showed wrong feature state of two. Similarly, it is there in between 25 and 30 and also at 35. This implies that all the four features had all the noisy sets at this particular data. Moreover, it can be inferred that the wrong classification goes either just one state above or just one state below and has never made a two-state jump which implies that the noisy data that belong to state one may show a wrong class of two but not three. This is because of the contribution from all the four feature sets. It is not probable that all four features would be noisy at the same time. Similarly, data at three may have a wrong class of two but not one. These noisy features are removed by the optimization of SVM. Two different SVM classifications were performed with four features for all machining conditions. The first classification was between GLCM features *diagonal moment* and *dissimilarity*; the second was between *second diagonal moment* and *homogeneity*. The SVM was trained using all the training data up to dull tool wear condition. The testing data consisted of two different time intervals T=21 min and T=30 min. At every time interval, five values of all features are available, out of which two are used for training and three are used for testing, and care has been taken to avoid the merging of training and testing data. The mean of all three test values is taken as test data to be classified. This eliminated any noisy data out of the three test data

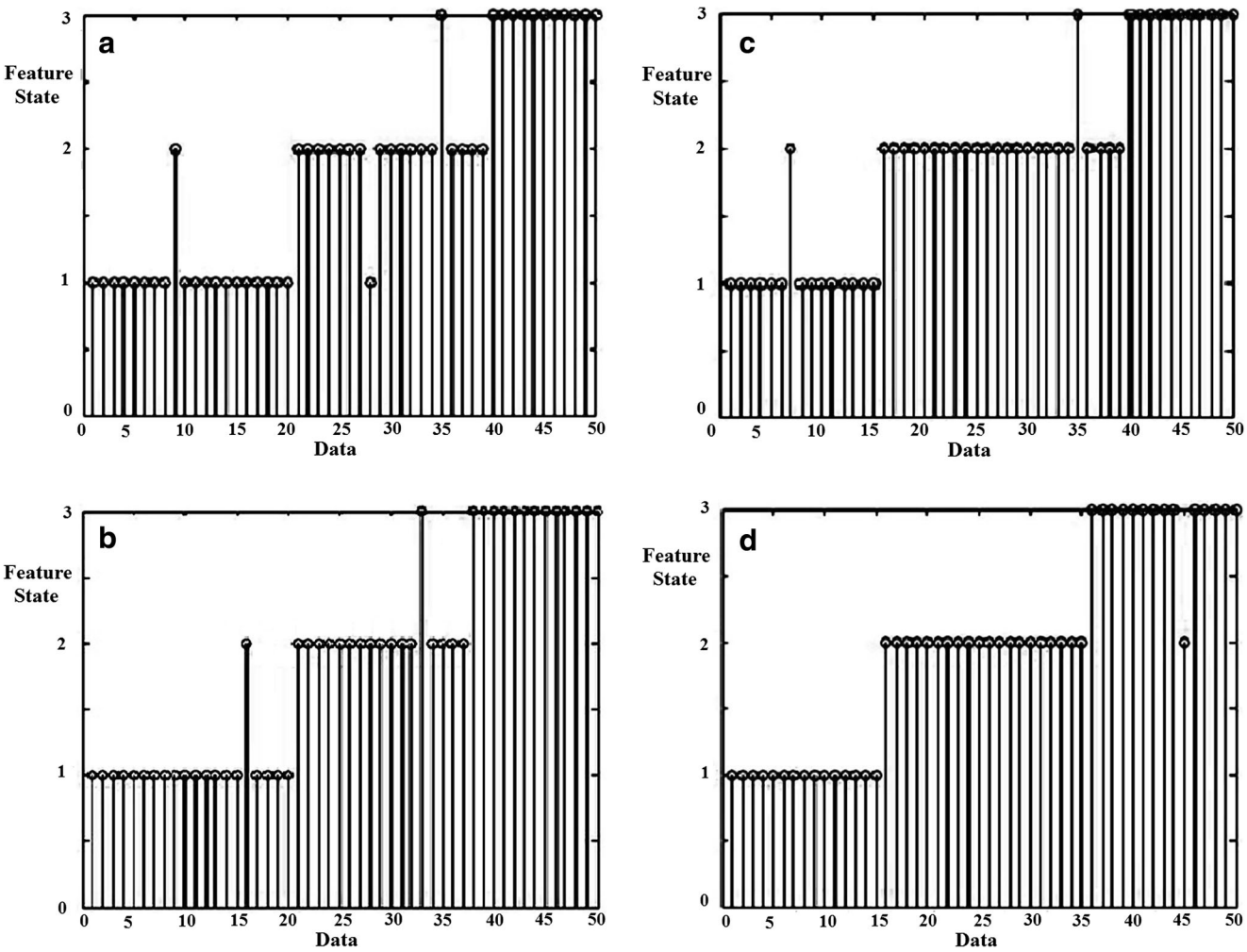

Fig. 6 **a** Feature state plot for M1, **b** feature state plot for M2, **c** feature state plot for M3, and **d** feature state plot for M4

Table 7 Classification efficiency for Gaussian and polynomial kernel

Machining condition	Gaussian kernel (% classification efficiency)		Polynomial kernel (% classification efficiency)	
	Diagm versus Dis	SDiagm versus Homo	Diagm versus Dis	SDiagm versus Homo
M1 training	86	86	99	99
Testing	80	80	96	96
M2 training	82	82	98	98
Testing	80	80	95	95
M3 training	77	77	96	96
Testing	74.5	74.5	94	94
M4 training	84	84	99	99
Testing	82	82	97	97

as the mean would always be close to the actual value, thus minimizing the chance of misclassification. The classification is carried out using two different sets of kernels, Gaussian and polynomial kernels (with 7, 8, and 9 degrees of polynomials). For multi-classification, a one versus one method is used. Table 7 shows the

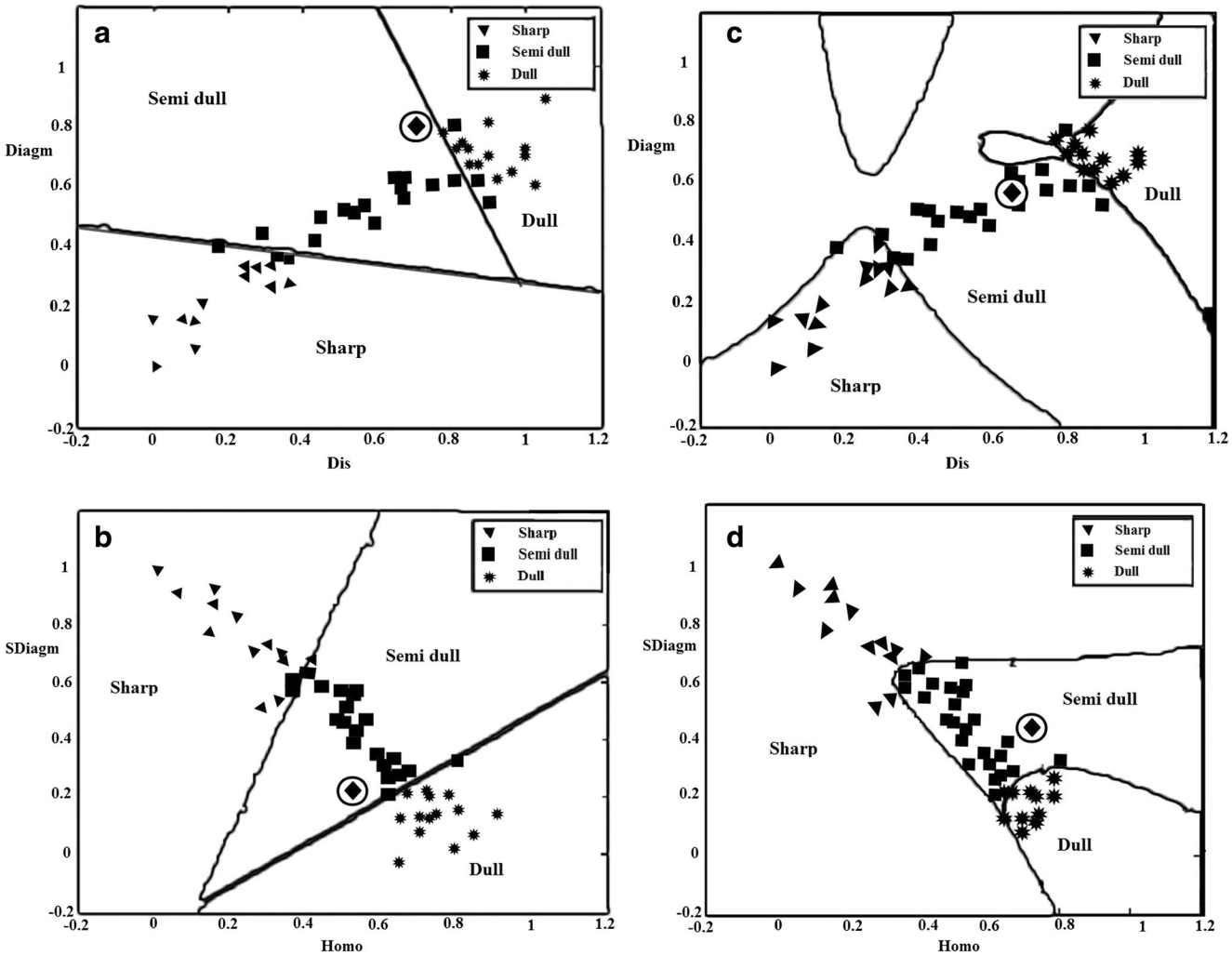

Fig. 7 **a** Diagm versus Dis for Gaussian kernel at T=21 min for M1, **b** SDiagm versus Homo for Gaussian kernel at T=21 min for M1, **c** Diagm versus Dis for polynomial kernel at T=21 min for M1, and **d** SDiagm versus Homo for polynomial kernel at T=21 min for M1

results of classification efficiency for Gaussian and polynomial kernels. Training and testing data are classified by both kernels for all four machining conditions.

From Table 7 it is found that polynomial kernel shows better consistency than the Gaussian kernel, which implies that the GLCM features of tool wear response follow a polynomial behavior than Gaussian. Classification results for Gaussian and polynomial kernels for machining condition M1 at T=21 min are shown in Fig. 7a, b, c, d. Figure 8a, b, c, d shows the results of classification of Gaussian and polynomial kernels for machining condition M2 at T=30 min.

In the above images, the area where the triangle markers ("▼") belong is the sharp tool condition, the area of square markers ("■") represents semi-dull condition, and the star marker points ("*") represent the dull tool condition data. The diamond marker ("♦") indicates the unknown data point at T=21 min/T=30 min, respectively.

5 Conclusion

Condition monitoring of uncoated carbide tool for turning of a medium carbon steel workpiece has been performed by processing the machined surface images using the GLCM technique. Fifteen features have been extracted from the GLCM of machine surface images. FDR analysis has been performed for feature selection. Observation of the results concludes that among all 15 features, *diagonal moment*, *second diagonal moment*, *dissimilarity*, and *homogeneity* are selected features to describe the tool condition. Then, the SVM classification technique using Gaussian and polynomial kernels has been utilized to classify sharp, semi-dull, and dull tool. Polynomial kernel (degree 7, 7, or 9) can be chosen for its higher efficiency. The method for tool condition monitoring applied in the study is a noninvasive and flexible technique which may be used for online tool condition monitoring purpose.

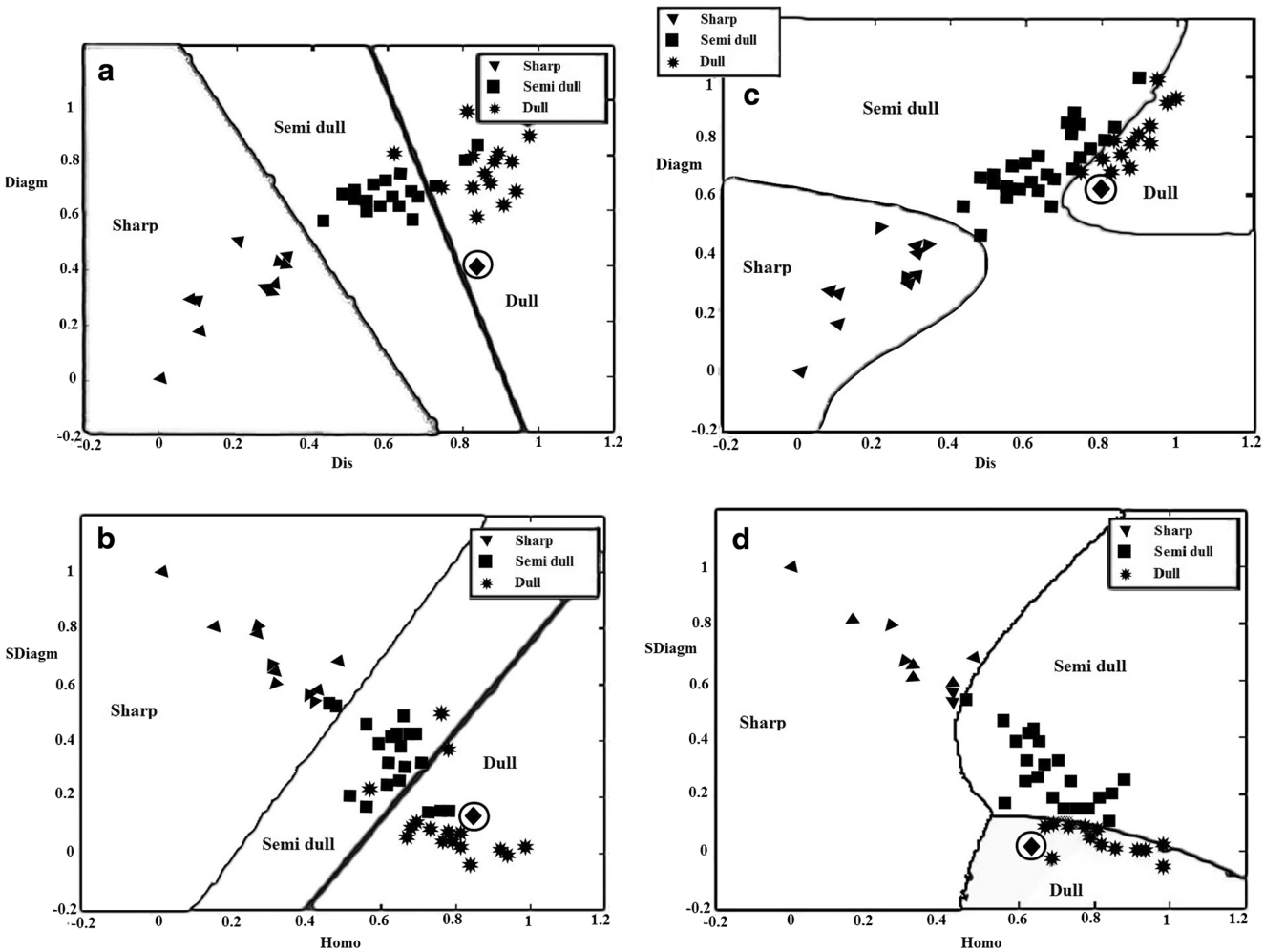

Fig. 8 **a** Diagm versus Dis for Gaussian kernel at T=30 min for M2, **b** SDiagm versus Homo for Gaussian kernel at T=30 min for M2, **c** Diagm versus Dis for polynomial kernel at T=30 min for M2, and **d** SDiagm versus Homo for polynomial kernel at T=30 min for M2

References

1. Byrne G, Dornfeld D, Inasaki I, Ketteler G, König W, Teti R (1995) Tool condition monitoring (TCM) – the status of research and industrial application. Ann CIRP 44/2:541–568
2. Mannan MA, Kassim AA, Jing M (2000) Application of image and sound analysis techniques to monitor the condition of cutting tools. Pattern Recogn Lett 21:969–9793
3. Dutta S, Pal SK, Mukhopadhyay S, Sen R (2013) Application of digital image processing in tool condition monitoring: a review. CIRP J Manuf Sci Technol 6:212–232
4. Kassim AA, Mannan MA, Jing M (2000) Machine tool condition monitoring using workpiece surface texture analysis. Mach Vis Appl 11:257–263
5. Bradley C, Wong YS (2001) Surface texture indicators of tool wear – a machine vision approach. Int J Adv Manuf Technol 17:435–443
6. Kang MC, Kim JS, Kim KH (2005) Fractal dimension analysis of machined surface depending on coated tool wear. Surf Coat Technol 193:259–265
7. Dhanasekar B, Krishna MN, Bhaduri B, Ramamoorthy B (2008) Evaluation of surface roughness based on monochromatic speckle correlation using image processing. Precis Eng 32:196–206
8. Dutta S, Kanwat A, Pal SK, Sen R (2013) Correlation study of tool flank wear with machined surface texture in end milling. Measurement 46:4249–4260
9. Datta A, Dutta S, Pal SK, Sen R (2013) Progressive cutting tool wear detection from machined surface images using Voronoi tessellation method. J Mater Process Technol 213:2339–2349
10. Wong FS, Nee AFC, Li XQ, Reisdorj C (1997) Tool condition monitoring using laser scatter pattern. J Mater Process Technol 63:205–210
11. Ho SY, Lee KC, Chen SS, Ho SJ (2002) Accurate modelling and prediction of surface roughness by computer vision in turning operations using an adaptive neuro-fuzzy inference system. Int J Mach Tools Manuf 42:1441–1446
12. Lee BY, Yu SF, Juan H (2004) The model of surface roughness inspection by vision system in turning. Mechatronics 14:129–141
13. Kumar R, Kulashekar P, Dhanasekar B, Ramamoorthy B (2005) Application of digital image magnification for surface roughness evaluation using machine vision. Int J Mach Tools Manuf 45:228–234
14. Al-Kindi GA, Shirinzadeh B (2007) An evaluation of surface roughness parameters measurement using vision-based data. Int J Mach Tools Manuf 47:697–708
15. Ramamoorthy B, Radhakrishnan V (1993) Statistical approaches to surface texture classification. Wear 167:155–161
16. Ramana KV, Ramamoorthy B (1996) Statistical methods to compare the texture features of machined surfaces. Pattern Recogn 29: 1447–1459
17. Datta A, Dutta S, Pal SK, Sen R, Mukhopadhyay S (2012) Texture analysis of turned surfaces using grey level co-occurrence technique. Adv Mater Res 365:38–43
18. Dutta S, Datta A, Das Chakladar N, Pal SK, Mukhopadhyay S, Sen R (2012) Detection of tool condition from the turned surface images using an accurate grey level co-occurrence technique. Precis Eng 36:458–466
19. Dutta S, Pal SK, Sen R (2014) Digital image processing in machining. In: Davim JP (ed) Modern, mechanical engineering - research development and education, 1st edn. Springer-Verlag, Berlin, pp 369–412
20. Chryssolouris G (1988) Sensor integration for tool wear estimation in machining. Sensor Control Manuf 1988:115–123
21. Rangwala S, Dornfeld DA (1990) Sensor integration using neural networks for intelligent tool condition monitoring. Trans ASME- J Eng Ind 112:219–228
22. Chryssolouris G (1992) Sensor synthesis for control of manufacturing process. Trans ASME- J Eng Ind 114:158–174
23. Tsai DM, Chen JJ, Chert JF (1998) A vision system for surface roughness assessment using neural networks. Int J Adv Manuf Technol 14:412–422
24. Du R, Elbestawi MA, Wu SM (1995) Automated monitoring of manufacturing processes, part 2: applications. J Manuf Sci Eng 117:133–141
25. Hirotoshi H et al (1993) Monitoring of milling process with an acoustic emission sensor. J Japan Soc Precis Eng 59:269–274
26. Leem CS, Dornfeld DA (1995) A customized neural network for sensor fusion in online monitoring of cutting tool wear. Trans ASME-J Eng Ind 117:152–159
27. Dong J, Hong GS, Wong YS (2004) Bayesian support vector regression for tool condition monitoring and feature selection. http://www.icsc.ab.ca/conferences/eis2004/conf/41.pdf. Accessed 30 October 2012
28. Sun J, Hong GS, Rahman M, Wong YS (2004) The application of nonstandard support vector machine in tool condition monitoring system. In: Proceedings of the Second IEEE International Workshop on Electronic Design, Test and Applications (DELTA'04). IEEE Computer Society Washington, DC, USA, 295–300. doi:10.1109/DELTA.2004.10017
29. Sun J, Rahman M, Wong YS, Hong GS (2004) Multiclassification of tool wear with support vector machine by manufacturing loss consideration. Int J Mach Tools Manuf 44:1179–1187
30. Cho S, Asfour S, Onar A, Kaundinya N (2005) Tool breakage detection using support vector machine learning in a milling process. Int J Mach Tools Manuf 45:241–249
31. Bhattacharyya P, Sanadhya SK (2006) Support vector regression based tool wear assessment in face milling. In: Proceedings of IEEE international conference on industrial technology. IEEE, New York, 2468–2473. doi:10.1109/ICIT.2006.372659
32. Sun J, Wong YS, Rahman M, Hong GS (2007) Identification of feature set for effective tool condition monitoring by acoustic emission sensing. Int J Prod Res 42:901–918
33. Shi D, Gindy NN (2007) Tool wear predictive model based on least squares support vector machines. Mech Syst Signal Process 21: 1799–1814
34. Salgado DR, Alonso FJ (2007) An approach based on current and sound signals for in-process tool wear monitoring. Int J Mach Tools Manuf 47:2140–2152
35. Hsueh YW, Yang CY (2008) Prediction of tool breakage in face milling using support vector machine. Int J Adv Manuf Technol 37: 872–880
36. Chiu NH, Guao YY (2008) State classification of CBN grinding with support vector machine. J Mater Process Technol 201: 601–605
37. Karacal C, Cho S, Yu W (2009) A novel approach to optimal cutting tool replacement. World Acad Sci Eng Technol 57:19–23
38. Jiang Z (2010) Intelligent prediction of surface roughness of milling aluminium alloy based on least square support vector machine. In: Cao H, Zhu X (eds) Proceedings of 2010 Chinese Control and Decision Conference, IEEE Industrial Electronics (IE) Chapter, Singapore, pp 2872–2876. doi:10.1109/CCDC.2010.5498687
39. Cho S, Binsaeid S, Asfour S (2010) Design of multisensor fusion-based tool condition monitoring system in end milling. Int J Adv Manuf Technol 46:681–694
40. Huang S, Li X, Gan OP (2010) Tool wear estimation using support vector machines in ball-nose end milling. https://www.phmsociety.

org/sites/phmsociety.org/files/phm_submission/2010/phmc_10_016.pdf. Accessed 1 October 2012
41. Elangovan M, Sugumaran V, Ramachandran KI, Ravikumar S (2011) Effect of SVM kernel functions on classification of vibration signals of a single point cutting tool. Exp Syst Appl 38: 15202–15207
42. Brezak D, Majetic D, Udiljak T, Kasac J (2012) Tool wear estimation using an analytic fuzzy classifier and support vector machines. J Intell Manuf 23:797–809
43. Çaydaş U, Ekici S (2012) Support vector machines models for surface roughness prediction in CNC turning of AISI 304 austenitic stainless steel. J Intell Manuf 23:639–650
44. Eddaoudi F, Regragui F, Mahmoudi A (2011) Masses detection using SVM classifier based on textures analysis. Appl Math Sci 5:367–379
45. Rode KN, Patil RT (2012) Texture analysis of MRI using SVM & ANN for multiple sclerosis patients. Int J Eng Res Appl 2: 1925–1928
46. Paneque-Gálvez et al. (2011) Textural classification of land cover using support vector machines: an empirical comparison with parametric, non parametric and hybrid classifiers in the Bolivian Amazon. http://heller.brandeis.edu/sustainable-international-development/tsimane/wp/TAPS-WP-69.pdf. Accessed 2 December 2012
47. Pawade PW, Suralkar SR, Karode AH (2012) Texture image classification using support vector machine. Int J Comput Technol Appl 3:71–75
48. Astakhov VP (2004) The assessment of cutting tool wear. Int J Mach Tools Manuf 44:637–647
49. Gonzalez RC, Woods RE (2002) Digital image processing. Prentice-Hall, New Jersey
50. Zuiderveld K (1994) Contrast limited adaptive histogram equalization. In: Heckbart PS (ed) Graphics gems IV. Academic Press Professional, California, pp. 474–485
51. Haralick RM, Shanmugam K, Dinsten I (1973) Textural features for image classification. IEEE Trans Syst SMC-3:610–621
52. Conners RW, Trivedi MM, Harlow CA (1984) Segmentation of a high resolution urban scene using texture operators. Comput Vis Graphics Image Process 25:273–310
53. Gadelmawla ES, Eladawi AE, Abouelatta OB, Elewa IM (2008) Investigation of the cutting conditions in milling operations using image texture features. Proc Inst Mech Eng B—J Eng Manuf 222: 1395–1404
54. Theodoridis S, Koutroumbas K (2009) An introduction to pattern recognition. Academic Press, Burlington
55. Chiang LH, Russell EL, Braatz RD (2000) Fault diagnosis in chemical processes using Fisher discriminant analysis, discriminant partial least squares and principal component analysis. Chemometr Intell Lab 50:243–252
56. Cristianini N, Shawe-Taylor J (2000) An introduction to support vector machines and other kernel-based learning. Cambridge University Press, Cambridge